PCCP

Cite this: Phys. Chem. Chem. Phys., 2012, 14, 7051–7058

www.rsc.org/pccp

PAPER

Giant piezoelectric resistance effect of nanoscale zinc oxide tunnel junctions: first principles simulations

Genghong Zhang,[a] Xin Luo,[ab] Yue Zheng*[a] and Biao Wang*[a]

Received 20th November 2011, Accepted 14th March 2012
DOI: 10.1039/c2cp23652d

Based on first principles simulations and quantum transport calculations, we have investigated in the present work the effect of the mechanical load on transport characteristics and the relative physical properties of nanoscale zinc oxide (ZnO) tunnel junctions, and verified an intrinsic giant piezoelectric resistance (GPR) effect. Our results show that the transport-relevant properties, *e.g.*, the piezoelectric potential (piezopotential), built-in electric field, conduction band offset and electron transmission probability of the junction *etc.*, can obviously be tuned by the applied strain. Accordingly, it is inspiring to find that the current–voltage characteristics and tunneling electro-resistance of the ZnO tunnel junction can significantly be adjusted with the strain. When the applied strain switches from −5% to 5%, an increase of more than 14 times in the tunneling current at a bias voltage of 1.1 V can be obtained. Meanwhile, an increase of up to 2000% of the electro-resistance ratio with respect to the zero strain state can be reached at the same bias voltage and with a 5% compression. According to our investigations, the giant piezoelectric resistance effect of nanoscale ZnO tunnel junctions exhibits great potential in exploiting tunable electronic devices. Furthermore, the methodology of strain engineering revealed in this work may shed light on the mechanical manipulations of electronic devices.

I. Introduction

Since the room-temperature ultraviolet laser emission of zinc oxide (ZnO) microcrystalline thin film was reported in the late twentieth century,[1] research on ZnO has attracted much attention and this has been increasing over the last ten years. Because of its unique nature of being both semiconducting and piezoelectric, ZnO has been extensively explored as an important functional material exhibiting outstanding mechanical, electrical and optical performances. For example, ZnO is widely used in various applications, such as ultraviolet light emitting and detection devices,[2,3] solar cells,[4] laser diodes[5] and thin film transistors,[6] *etc*. In particular, with the development of nanotechnology in synthesis and characterization processes, a variety of ZnO nanostructures, such as nanowires, nanotubes, nanobelts, nanorings and nanocombs, have been successfully synthesized.[7] These high-quality ZnO nanostructures can be used as building blocks to assemble functional nanodevices. With the coupling of unique bulk properties, surface and interface effects, ZnO nanodevices exhibit various novel properties, which can be exploited to design nanogenerators,[8] piezoelectric field-effect transistors[9,10] and nanoforce sensors,[10] *etc*., and have potential applications in electronics, optoelectronics, sensors and biological sciences.[11]

Most applications of ZnO functional devices are involved with metal/ZnO interfaces. Therefore, it is essential to understand the physics at metal/ZnO interfaces and the effect of these interfaces on the device performances. Using first principles calculations based on density functional theory, Dong and Brillson[12] have shown that the interfacial bonding environment has a significant effect on the Schottky barrier heights. Kamiya *et al.*[13] investigated the interfacial electronic structure and carrier transport properties of ZnO sandwiched between metals, and found that the Au/ZnO interface formed a Schottky contact and the Mg/ZnO interface formed an Ohmic contact. More recently, the electron transport of ZnO nanowires coupled with Al electrodes have been studied by Yang *et al.*,[14] who found that the contact interfaces play important roles in charge transport.

In practical fabrication processes and applications involving heterostructure-based functional devices it is difficult to avoid strain effect, which could be introduced by heteroepitaxy, defects, and external clamping or loading. In particular for ZnO tunnel junctions, due to the piezoelectric nature of ZnO, it is crucial to consider the strain effect on the mechanical and electronic properties of the junctions. The existence of strain would definitely change the properties of the tunnel junctions,

[a] *State Key Laboratory of Optoelectronic Materials and Technologies/ Institute of Optoelectronic and Functional Composite Materials, Micro-Nano Physics and Mechanics Research Laboratory, School of Physics and Engineering, Sun Yat-sen University, Guangzhou 510275, China. E-mail: zhengy35@mail.sysu.edu.cn, wangbiao@mail.sysu.edu.cn*
[b] *Institute of High Performance Computing, 1 Fusionopolis Way, #16-16 Connexis, 138632, Singapore*

especially the interfacial electronic structures and other transport-related properties. For example, Zheng *et al.* proposed to tune the tunneling electro-resistance of ferro-electric tunnel junctions through the mechanical loads, which has been verified using first principles simulations by Luo *et al.*[15,16] Recently, Zhang *et al.*[17] presented a study on the effect of deformation induced piezopotential spatial distribution on the local charge transport property of a ZnO micro/nanowire combining finite element simulations and experimental examinations. Coupling the piezoelectricity with semiconductor characteristic of ZnO, Wang[18,19] investigated manipulations on the carrier transport behavior in ZnO nanowires/nanobelts utilizing the strain dependent piezo-potential and has fabricated various electronic components and devices experimentally. Nevertheless, the strain effect on the transport characteristics and relative electronic properties of ZnO tunnel junctions has not yet been systematically investigated based on first principles simulations.

To gain more insight into the transport characteristics of nanoscale ZnO tunnel junctions and perform strain manipulations on it, we present an investigation on Ag–ZnO–Ag tunnel junctions using first principles quantum transport calculations. Combining density functional theory with the nonequilibrium Green function's (NGF) approach, the strain effect on transport and other electronic properties of the ZnO tunnel junction, including electrostatic potential profile, built-in electric field, local density of states (LDOS), transmission spectra and current–voltage response, *etc.*, is studied. The giant piezoelectric resistance (GPR) effect of the ZnO tunnel junctions has been comprehensively discussed.

II. Simulation methods

In the following simulations, the atomic structure of the Ag–ZnO–Ag tunnel junction is schematically shown in Fig. 1. In this two-probe system, periodic boundary condition is applied in the plane (x-y plane) perpendicular to the transport direction (z direction). The system is divided into three regions, *i.e.* the left electrode, the right electrode and the central scattering region. Four and three Ag layers are included in the scattering region at the left and right sides in order to screen the influence of the ZnO barrier on the electrode regions. Considering the crystal structures of ZnO (hexagonal structure) and Ag (face central cubic structure) and their atom stacking manners (both close-packing with different atom stacking sequences described as ABAB and ABCABC for ZnO and Ag (111) plane, respectively), we choose here Ag (111) and ZnO (0001) planes as the building blocks to construct the tunnel junction. According to the previous treatments,[12,13] the unit cell lattice parameters of the junction in the x-y plane are taken to be the same as those of ZnO since Ag electrodes are more flexible. The external applied strain is exerted along the directions of the in-plane lattice basic vectors, *i.e.*, the directions of **a** and **b**, as shown in Fig. 1(c). Here, the tensile strain is defined as positive, whilst the compressive strain is defined as negative.

In this work, all the constructed two-probe structures at each given in-plane strain are relaxed and optimized using the Vienna *Ab initio* Simulation Package (VASP),[20,21] which is based on density functional theory (DFT) and uses plane wave basis sets. The projector-augmented wave method (PAW) is used here and the exchange correlation potentials are treated by the Perdew–Burke–Ernzerhof (PBE) parameterization within the generalized gradient approximation (GGA).[22–24] A $9 \times 9 \times 3$ k-point mesh for the two-probe system relaxation is used in the Brillouin zone according to the Monkhorst–Pack method.[25] The tetrahedron method with Blöchl corrections is employed. To improve accuracy, the energy cutoff of the plane wave basis set is applied up to 500 eV. The relaxation at each given strain consists of the following steps. We first respectively

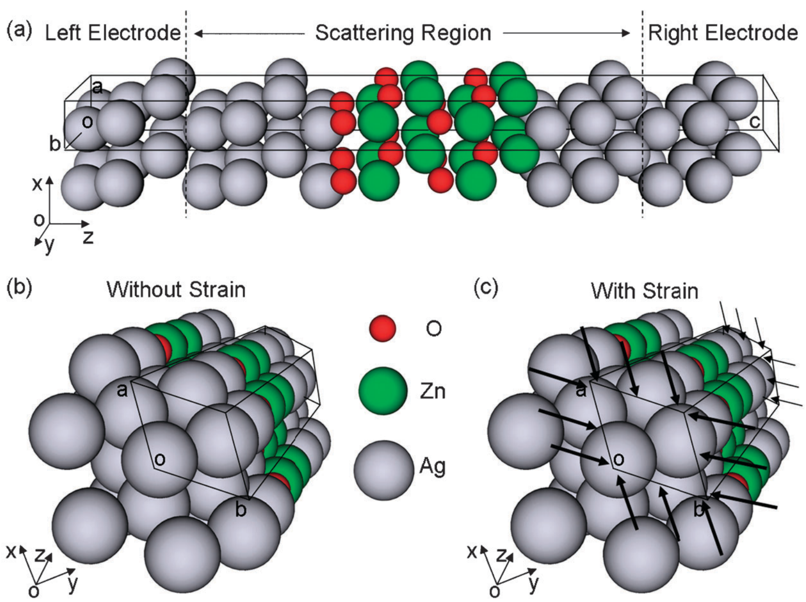

Fig. 1 (a) Schematic atomic structure of the Ag–ZnO–Ag tunnel junction. The box shows the unit cell of the system. (b) Top view of the junction. (c) Scheme of how strain is exerted to the junction. Strain is parallel to the in-plane lattice basic vectors, **a** and **b**.

relax the bulk ZnO and bulk Ag under the in-plane lattice constraint. Using these resulting lattice constants and building blocks we then construct the ZnO tunnel junction and optimize the interfacial layer distances between ZnO barrier and Ag electrodes. Lastly the constructed two-probe system is fully relaxed to obtain the optimized structure.

To demonstrate the effect of the applied strain on electron transport of the ZnO tunnel junction, we use the Atomistic Toolkit package (ATK),[26,27] which combines NGF technique with DFT calculations,[28] to investigate the transport behavior of the Ag–ZnO–Ag two-probe system under different strain conditions. Exchange correlation potentials with Perdew–Burke–Ernzerhof parameterization of the generalized gradient approximation (GGA.PBE) are used. To ensure accuracy, the localized numerical atomic orbital basis set for all atoms in the system is set to be double zeta polarized. The Brillouin zone of the system is sampled by an $18 \times 18 \times 100$ k-point mesh for the self-consistent calculations and an up to 300×300 mesh is chosen for the 2D $K_{\parallel}$ resolved electron transmission calculations to assure convergence. To calculate the tunneling current, a 70×70 k-point mesh sampling is used for integrating the transmission spectrum in the 2D Brillouin zone perpendicular to the transport direction.

III. Results and discussions

A. Strain adjusting electrostatic potential and LDOS of the ZnO tunnel junction

For the Ag–ZnO–Ag tunnel junction, the interfacial bonding at the two Ag/ZnO interfaces is asymmetric. Therefore, a polarization is expected in the ZnO barrier due to its dissimilar polar surfaces, which would produce a built-in electric field across the barrier. To verify this, we calculate the electrostatic potential energy of the unstrained tunnel junction along the z direction under zero bias (see Fig. 2(a)). Since the Ag–ZnO–Ag junction is lattice-mismatched along the z direction, we adopt the double-macroscopic-average method to smooth the planar-averaged potential energy obtained by taking a planar average integration of the three dimensional potential energy profile in the x-y plane.[29,30] From Fig. 2(a), it can be seen that there are obvious distortions of the potential energy near both interfaces due to interactions between electrodes and the ZnO barrier. Nevertheless, it is easy to find the potential drop across the ZnO barrier. By linear fitting the potential energy profile of the ZnO barrier away from the interfaces, we estimate the polar surfaces induced built-in electric field across the barrier to be about 1.9 V nm^{-1}. As it will be shown in the following, this electric field will result in diode-like behavior of the current–voltage curve.

In the present work we would like to see how the applied strain affects the potential profile and the built-in electric field of the ZnO barrier. For comparison of different strain conditions, we choose the potential energy at the center of the ZnO barrier as the zero potential energy point. As shown in Fig. 2(b) it can be seen that the potential profile within the ZnO barrier is sensitive to the applied strain. The slope of the potential energy in the central ZnO region is obviously changed under different strain conditions. The resulting built-in electric fields within ZnO barrier at strains of -4%, 0% and 4% are 1.7 V nm^{-1}, 1.9 V nm^{-1} and 2.0 V nm^{-1}, respectively. Owing to the exponential dependence of the tunneling current on potential energy, we consider it as a quite remarkable adjustment. Furthermore, relative to the dissimilar polar surfaces induced potential drop of the barrier without strain, we can also see that the potential rises near the left interface and the potential decreases near the right interface under tensile strain, whereas the potential decreases to the left and it rises to the right under compressive strain, which implies a strain dependent reversal of a certain potential which is the difference between the potential drops of the ZnO barrier with and without strain. Actually, this reversible potential is the piezopotential due to the piezoelectric effect of ZnO,[31] which also results in a reversible strain induced built-in electric field. Consequently, the above calculated potential within the ZnO barrier under strain is comprised of the dissimilar polar surfaces induced potential and the reversible strain dependent piezopotential. Accordingly, the calculated built-in electric field is the total electric field induced by the above two potentials.

It has been reported that the conduction band would shift towards a higher level of energy and the band gap would become wider in bulk ZnO when the applied hydrostatic pressure on ZnO increases.[32] To gain insight into the influence of the in-plane strain on the electronic structure of the ZnO tunnel junction, we calculate the local density of states (LDOS) of the junction under different strains as shown in Fig. 2(c). As depicted by the dot line, the Fermi level is set to zero. The left and right Ag electrodes are labeled as LE and RE, respectively. Results indicate that the LDOSs with different strains exhibit similar tendencies. It can be seen that, due to the built-in electric field, the valence band edges of the ZnO layers gradually depart from the Fermi level from the left electrode to the right electrode. Further analysis shows that the interfacial interaction has an effect on the interfacial LDOS. Due to the hybridization between the polar surfaces of the ZnO barrier and the adjacent Ag electrode layers, some new hybrid peaks appear in the LDOS at the interfacial Ag layers. As depicted by the arrows in Fig. 2(c), we can see that conduction band tends to shift ($\sim$2eV) towards a higher level of energy when the applied in-plane strain switches from tension (4%) to compression (-4%), which can be attributed to the piezoresistance effect of the ZnO barrier (treated as a body effect).[33] Due to the thinness of the ZnO barrier and the interface interaction, it is not very clear to see the band offset, especially for the outermost ZnO layers. However, it should be more significant when the ZnO barrier is thick enough.

B. Strain controlling electron transport of the ZnO tunnel junction

From what we have discussed above, we can see that the applied strain effectively influences the electrical properties of the ZnO tunnel junction, *i.e.*, the piezoelectric effect on the piezopotential and the piezoresistance effect on conduction band offset, which should have great impact on electron transport. The calculated transmission spectra of the tunnel junction under strains of -4%, 0% and 4% are depicted in Fig. 3(a). It can be seen that for each transmission spectrum

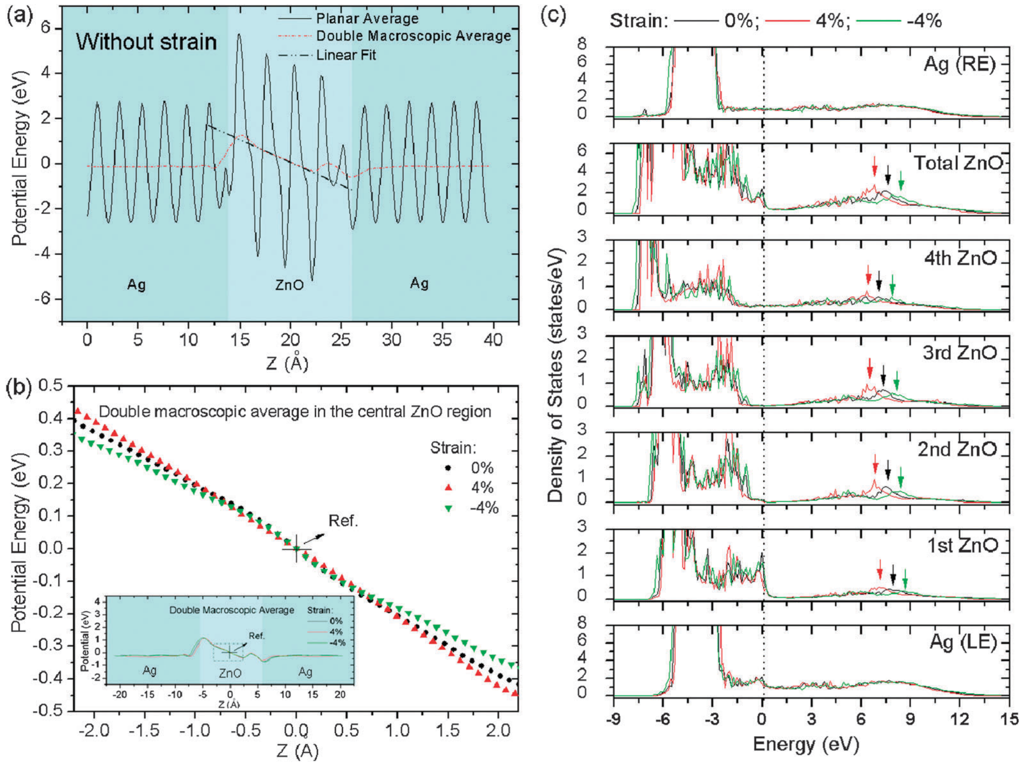

Fig. 2 (a) The calculated electrostatic potential energy profile of the junction without strain and (b) the double macroscopic averages (DMAs) of the potential energy under different strains near the center of the ZnO barrier. The insert in (b) depicts average potential energy profiles of the whole junction under different strains. (c) The local density of the states (LDOS) of the junctions under different strains. The arrows mark out the peaks of the conduction bands of the junctions under different strains.

there is a transmission valley near the Fermi level, which coincides with the band gap in the LDOS. It is the electrons having energy in this zone which contribute most to the tunneling current when the bias voltage is not too large. From comparison of the transmission spectra, it clearly shows that the in-plane strain indeed affects the transmission probability of electrons, especially those near to the Fermi level. The transmission probability near the Fermi level gets enhanced when the applied strain changes from compression to tension, which is consistent with the conduction band shift in the LDOS. Meanwhile, further inspection shows that the total transmission integrated with overall energy also increases with the increasing strain, although some transmission disturbance appears at a moderate energy region in the transmission spectra which may be due to the open or close of some transmission channels there, or is relative to the localization change of electronic states in this region. To gain more insight into the strain effect on transmission, we also analyze the $K_{\parallel}$ resolved transmission by projecting the transmission at the Fermi level onto the 2D Brillouin zone perpendicular to the transport direction for the junctions under different strains, as shown in Fig. 3(b) 3(c) and 3(d). Results show that the main contribution to the Fermi level transmission comes from the region around the center of the Brillouin zone at Γ point ($K_{\parallel} = 0$) for all the junctions (note that here we only depict the $K_{\parallel}$ resolved transmission spectra in the central Brillouin zone with K_x and K_y ranging from −0.2 to 0.2). However, the transmission probability at this region increases remarkably when the applied strain changes from compressive (−4%) to tensile (4%). The transmission probability maximums in this zone are about 0.07, 0.25 and 0.60 for the junctions under strains of −4%, 0% and 4%, respectively. This remarkable change might originate from the decreasing scattering of electrons caused by the polar interfaces when the strain changes from compressive to tensile.

In the following, we would like to investigate the strain influence on the current transport behavior of the ZnO tunnel junction. The tunneling current across a two-probe system can be calculated as the overall energy integral of the transmission spectrum weighted by the Fermi distribution difference between the left and right electrodes at given energy, which can be expressed as the Landauer–Büttiker formula[34–36]

$$I = \frac{2e}{h}\int T(E)[f_{\mathrm{F}}(E-\mu_{\mathrm{L}}) - f_{\mathrm{F}}(E-\mu_{\mathrm{R}})]dE, \qquad (1)$$

where μ_{L} and μ_{R} are the chemical potentials of the left and right electrodes, respectively, $T(E)$ is the transmission probability function, and f_{F} is the Fermi distribution function.

The calculated tunneling current as a function of applied voltage for junctions under different strains is presented in Fig. 4(a). The inserted figure indicates the direction of the forward bias and the built-in electric field of the ZnO barrier. The positive direction of the bias voltage is defined when the bias applied to the left electrode is higher than that applied to the right one. Meanwhile, only half of the desired bias voltage is assigned to the left electrode whilst the remaining half bias

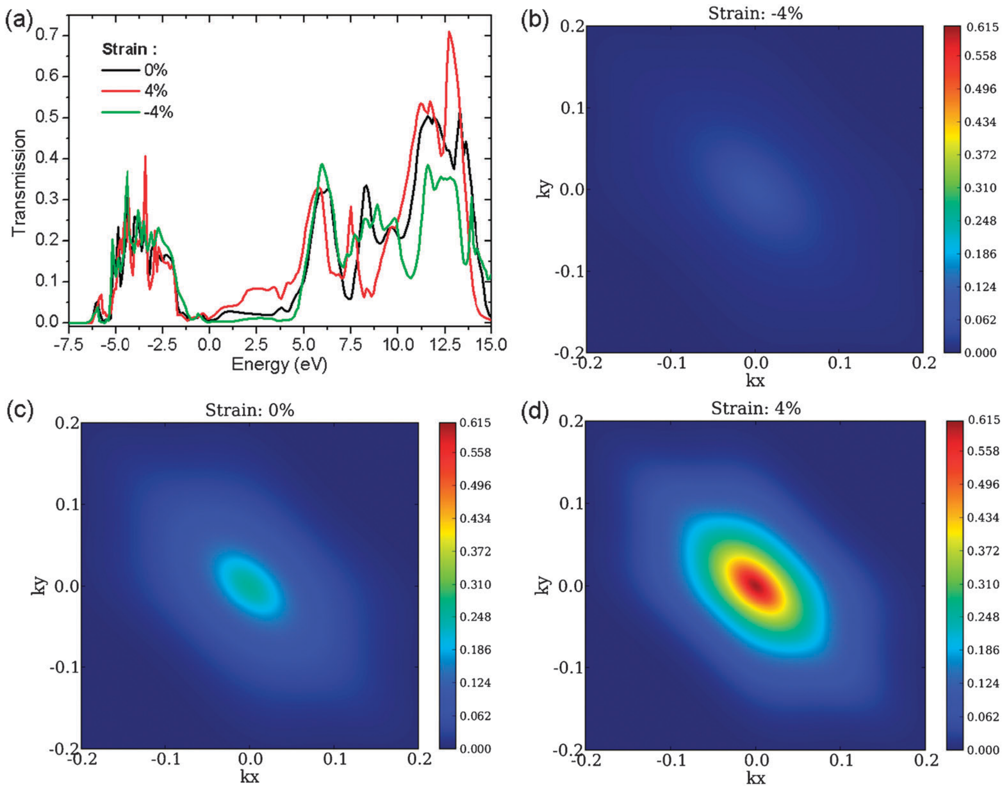

Fig. 3 (a) Dependence of the transmission spectra on the energy for junctions under different strains. The Fermi level is set to zero. $K_{\parallel}$ resolved transmission at the Fermi level for junctions under strains of (b) −4%, (c) 0% and (d) 4%.

voltage is assigned to the right one. It can be seen that all the current–voltage curves exhibit diode-like behavior. For the same magnitude of applied voltage, a larger current is obtained for the negative bias voltage. Meanwhile, nonlinearity of the current–voltage curves begins to appear when the bias is large enough, especially for the negative bias. The diode-like feature of the current–voltage curves is clearly due to the built-in electric field, which partially cancels out (enhances) the external field when positive (negative) bias voltage is applied. This feature is expected to be more apparent if we further break the symmetry of the junction, such as by choosing dissimilar electrodes. More importantly, the effect of in-plane strain on the current transport of the junction is quite remarkable. As shown in Fig. 4(a), with the strain changing from compression (−5%) to tension (5%), the tunneling current increases notably in the whole applied voltage range. To see this tuning effect more clearly, we also plot the tunneling current as a function of strain under different voltages, as shown in Fig. 4(b) and the insert. Note that in the main figure the magnitude of current has been rescaled by that of the junction under the largest compression, *i.e.* −5%. It can be seen that the tunneling current is quite sensitive to strain at a given bias voltage. The current ratio increases by about an order of magnitude as the strain increases from −5% to 5% when the magnitude of bias voltage is not too small (*i.e.*, larger than ∼ 0.3 V). Meanwhile, it increases more remarkably in larger magnitudes of bias voltage. At the 1.1 V positive bias voltage, we obtain a 14.4-times increase in current (from 0.11 μA to 1.58 μA) when the applied strain increases from −5% to 5%. Furthermore, the result also indicates that similar to the bias voltage, the strain effect on the current ratio is also nonlinear, manifesting an increasing sensitivity at larger strains. This result clearly indicates that we can obtain significant control on the current transport across the ZnO junction through strain engineering.

C. Giant piezoelectric resistance effect of the ZnO tunnel junction

To characterize the strain controllability on the tunneling electro-resistance (TER) of the junction, we calculate the TER of the ZnO junction as a function of bias voltage under different strains, as shown in Fig. 5(a). It can be seen that the TER strongly depends on bias voltage and strain, and that it is more sensitive to compressive strain and forward bias. We can clearly see an asymmetry of the resistance-voltage dependence due to the built-in electric field. More importantly, at a given bias voltage the TER is always increasing as strain changes from tension to compression, and the TER of junctions under compressive strain is much larger than that of junctions under tensile strain. To quantiatively characterize the strain-dependent TER effect, we have previously introduced a giant piezoelectric resistance (GPR) ratio which is a function of applied strain and can be defined as[15,16,37]

$$\mathrm{GPR} = \frac{R_s - R_0}{R_0}, \tag{2}$$

where R_s and R_0 are the electro-resistances of junctions with and without applied strain, respectively. From the definition, we can see that when $R_s \geq R_0$, a larger GPR ratio indicates a more significant strain manipulation. Meanwhile, when $R_s < R_0$, the strain manipulation is more remarkable when the GPR

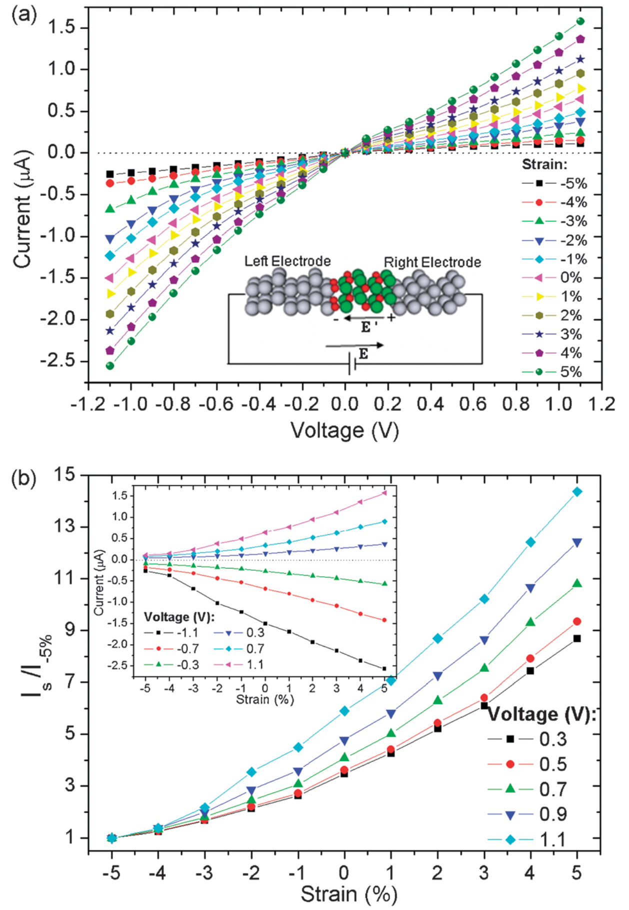

Fig. 4 (a) Tunneling current as a function of bias voltage of junctions under different strains. The insert depicts the loading method of the forward bias. The external and built-in electric fields are labeled as E and E', respectively. (b) The rescaled tunneling current as a function of applied strain at different bias voltages. The insert depicts the strain dependence of the tunneling current at different bias voltages.

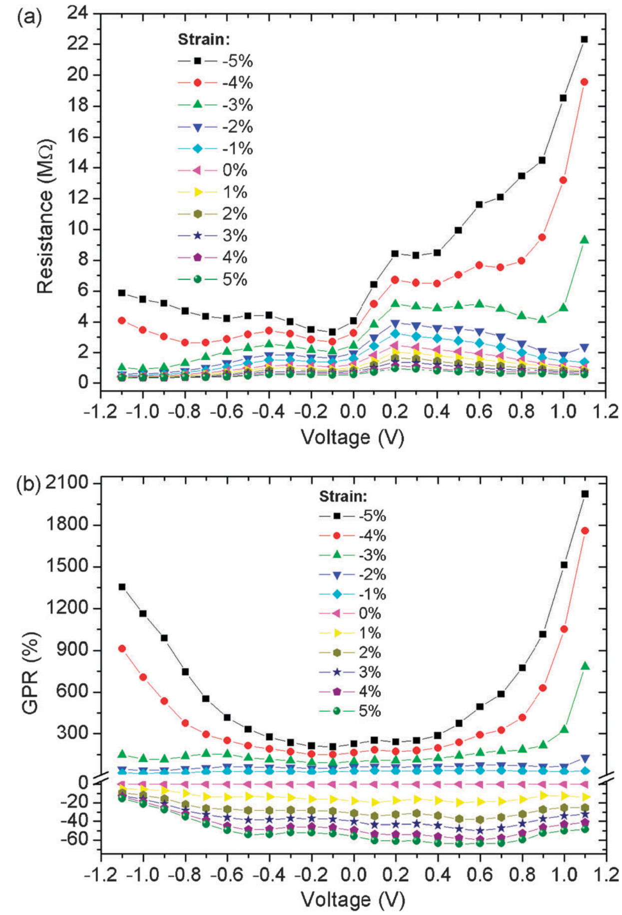

Fig. 5 (a) Tunneling electro-resistance as a function of bias voltage for junctions under different applied strains. (b) Dependence of the GPR ratio on bias voltage under different applied strains.

ratio is closer to −100%. Bearing this in mind, we investigated the GPR ratio of the junction as a function of applied bias under different strains, as shown in Fig. 5(b). It can be seen that the GPR ratio is not constant but dependent on bias voltage. In particular, the GPR ratio is very sensitive to applied bias when large compression is applied, manifested by a significant increase at the voltage boundaries. For example, with a compression of −5%, the GPR ratio of the tunnel junction can change from 252.3% to 2023.3% when the applied bias increases from 0.1 V to 1.1 V. However, the GPR ratio seems to be less relative with applied bias when the magnitude of the applied strain is small (*e.g.*, the strain is between −2% and 2%). Meanwhile, we can also see that the GPR ratio tends to decrease first and then increase as the absolute value of applied bias increases from zero with a large tensile strain. Especially, a minimal GPR of −63.9% is obtained at 0.5 V bias voltage and with a 5% tensile strain. From Fig. 5(b), we can also see that the GPR ratio is strongly dependent on the applied strain, indicating a strong GPR effect in ZnO tunnel junction. The similar behaviors have also been investigated by Wang *et al.*,[18,19,33] they defined this behavior, *i.e.*, piezotronic effect, as the effect of piezoelectric potential tuning to the charge transport at a metal-semiconductor interface or p–n junction.

To summarize the GPR effect of the ZnO tunnel junction, we also plot the dependence of GPR ratio on the applied strain under different bias voltages, see Fig. 6(a). We can see that the GPR ratio of the junction decreases monotonously with the increasing strain at each bias voltage, manifested by a large drop at the compression region. Moreover, it also shows that at larger given bias voltages the GPR effect of the junction is more significant. At 1.1 V bias voltage, the GPR ratio can change from −48.6% to 2023.3% when the applied strain changes from 5% to −5%. Generally, a larger magnitude of GPR ratio can be obtained in junction under larger magnitudes of strain, especially at a large bias for compression and at a moderate voltage for tension.

Finally, we would like to investigate the effect of the switching applied strain on the electro-resistance of the ZnO tunnel junction, which can be expressed as

$$\Phi_{\mp}(|s|) = R(-|s|)/R(+|s|), \tag{3}$$

that is, the tunneling electro-resistance ratio between two strain states $\mp|s|$ (compression and tension). The calculated $\Phi_{\mp}$ as a function of strain $|s|$ at different bias voltages is shown in Fig. 6(b). It can be seen that when the bias voltage is small

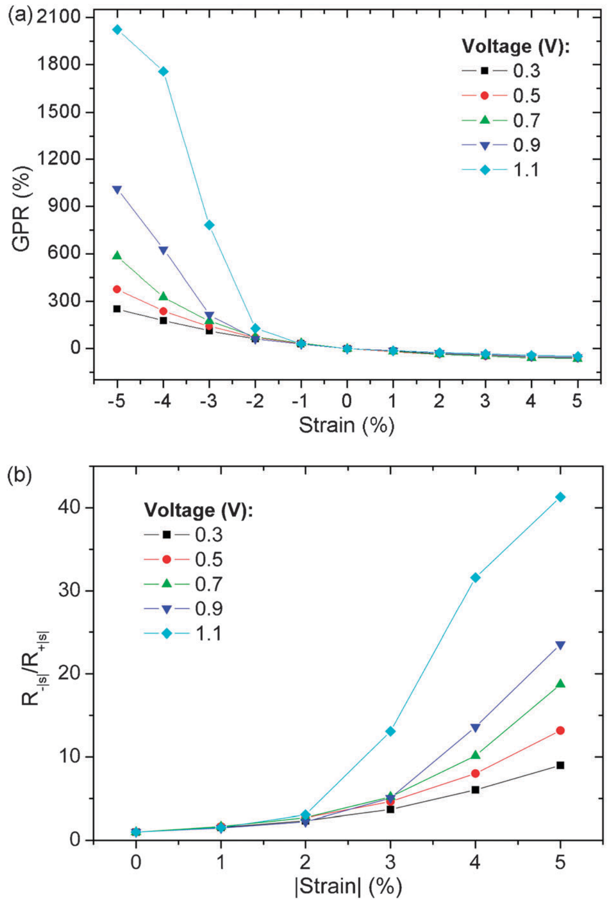

Fig. 6 (a) GPR ratio as a function of applied strain for junctions under different bias voltages. (b) Tunneling electro-resistance ratio between two strain states $\mp |s|$ as a function of strain magnitude $|s|$ at different bias voltages.

(*e.g.*, 0.3 V), $\Phi_{\mp}$ increases quite gently as the applied strain increases, and the increase becomes more and more significant at larger voltages, which is similar to the behavior of the GPR ratio. The ratio $\Phi_{\mp}$ is more than 40 at 1.1 V bias voltage with an absolute value of strain of 5%, indicating a remarkable change of the electro-resistance between the two strain states.

IV. Conclusions

In summary, the strain effect on the current transport behavior and relevant physical properties in nanoscale ZnO tunnel junctions is investigated using first principles calculations combined with the nonequilibrium Green's functions method. Our results show that the piezopotential, built-in electric field, conduction band offset and electron transmission probability of the Ag–ZnO–Ag tunnel junction can well be tuned by the external strain. As the applied strain switches from compression to tension, the piezopotential within ZnO barrier can be reversed, resulting in an obvious increase of the built-in electric field. Meanwhile, the conduction band of the ZnO barrier shifts towards a lower level of energy, and the electronic transmission probability nearby the Fermi level becomes larger. Most important of all, it is found that the response of current transport to the applied strain is quite sensitive. An increase of up to 14 times in the tunneling current is obtained when the applied strain switches from compression to tension at a bias voltage of 1.1 V. This behavior is defined as the giant piezoelectric resistance (GPR) effect. Moreover, the calculated GPR ratio can even reach up to 2023.3% with the switched strains from 0% to −5% at the same bias voltage. All of these results imply that the external strains indeed have a significant impact on the current transportation of the ZnO tunnel junction. We believe that this GPR effect in nanoscale ZnO tunnel junctions provides us with an alternative efficient means to exploit the outstanding mechanical and electronic properties of ZnO. These results also imply promising prospects in designing tunable electronic devices through strain engineering.

Acknowledgements

Helpful discussions with W. J. Chen and X. L. Zou are gratefully acknowledged. We also acknowledge the financial support of the National Natural Science Foundation of China (NSFC) (Nos. 10902128, 11072271, 51172291, 10972239), the Fundamental Research Funds for the Central Universities, New Century Excellent Talents in University, Research Fund for the Doctoral Program of Higher Education, and Fok Ying Tung Foundation.

References

1 Z. K. Tang, G. K. L. Wong, P. Yu, M. Kawasaki, A. Ohtomo, H. Koinuma and Y. Segawa, *Appl. Phys. Lett.*, 1998, **72**, 3270.
2 M. H. Huang, S. Mao, H. Feick, H. Q. Yan, Y. Y. Wu, H. Kind, E. Weber, R. Russo and P. D. Yang, *Science*, 2001, **292**, 1897.
3 S. N. Das, K. J. Moon, J. P. Kar, J. H. Choi, J. J. Xiong, T. I. Lee and J. M. Myoung, *Appl. Phys. Lett.*, 2010, **97**, 022103.
4 V. Kruefu, E. Peterson, C. Khantha, C. Siriwong, S. Phanichphant and D. L. Carroll, *Appl. Phys. Lett.*, 2010, **97**, 053302.
5 T. Aoki, Y. Hatanaka and D. C. Look, *Appl. Phys. Lett.*, 2000, **76**, 3257.
6 Y. Kwon, Y. Li, Y. W. Heo, M. Jones, P. H. Holloway, D. P. Norton, Z. V. Park and S. Li, *Appl. Phys. Lett.*, 2004, **84**, 2685.
7 Z. L. Wang, *J. Phys.: Condens. Matter*, 2004, **16**, R829.
8 Z. L. Wang and J. H. Song, *Science*, 2006, **312**, 242.
9 M. S. Arnold, P. Avouris, Z. W. Pan and Z. L. Wang, *J. Phys. Chem. B*, 2003, **107**, 659.
10 X. D. Wang, J. Zhou, J. H. Song, J. Liu, N. S. Xu and Z. L. Wang, *Nano Lett.*, 2006, **6**, 2768.
11 Z. L. Wang, *MaterialsToday*, 2007, **10**, 20.
12 Y. F. Dong and L. J. Brillson, *J. Electron. Mater.*, 2008, **37**, 743.
13 T. Kamiya, K. Tajima, K. Nomura, H. Yanagi and H. Hosono, *Phys. Status Solidi A*, 2008, **205**, 1929.
14 Z. J. Yang, L. H. Wan, Y. J. Yu, Y. D. Wei and J. Wang, *J. Appl. Phys.*, 2010, **108**, 033704.
15 Y. Zheng and C. H. Woo, *Nanotechnology*, 2009, **20**, 075401.
16 X. Luo, B. Wang and Y. Zheng, *ACS Nano*, 2011, **5**, 1649.
17 Y. Zhang, Y. F. Hu, S. Xiang and Z. L. Wang, *Appl. Phys. Lett.*, 2010, **97**, 033509.
18 Z. L. Wang, *Adv. Mater.*, 2007, **19**, 889.
19 Z. L. Wang, *Nano Today*, 2010, **5**, 540.
20 G. Kresse and J. Hafner, *Phys. Rev. B*, 1993, **48**, 13115.
21 G. Kresse and J. Furthmuller, *Phys. Rev. B*, 1996, **54**, 11169.
22 P. E. Blöchl, *Phys. Rev. B*, 1994, **50**, 17953.
23 G. Kresse and D. Joubert, *Phys. Rev. B*, 1999, **59**, 1758.
24 J. P. Perdew, K. Burke and M. Ernzerhof, *Phys. Rev. Lett.*, 1996, **77**, 3865.
25 H. J. Monkhorst and J. D. Pack, *Phys. Rev. B*, 1976, **13**, 5188.
26 M. Brandbyge, J. L. Mozos, P. Ordejon, J. Taylor and K. Stokbro, *Phys. Rev. B*, 2002, **65**, 165401.

27 J. M. Soler, E. Artacho, J. D. Gale, A. Garcia, J. Junquera, P. Ordejon and D. Sanchez-Portal, *J. Phys.: Condens. Matter*, 2002, **14**, 2745.
28 M. C. Payne, M. P. Teter, D. C. Allan, T. A. Arias and J. D. Joannopoulos, *Rev. Mod. Phys.*, 1992, **64**, 1045.
29 L. Colombo, R. Resta and S. Baroni, *Phys. Rev. B*, 1991, **44**, 5572.
30 J. Junquera, M. H. Cohen and K. M. Rabe, *J. Phys.: Condens. Matter*, 2007, **19**, 213203.
31 J. Zhou, P. Fei, Y. D. Gu, W. J. Mai, Y. F. Gao, R. S. Yang, G. Bao and Z. L. Wang, *Nano Lett.*, 2008, **8**, 3973.
32 F. C. Zhang, Z. H. Deng, J. N. Yun, J. F. Yan, W. H. Zhang and Z. Y. Zhang, *J. Funct. Mater.*, 2006, **7**, 1063.
33 Y. Zhang, Y. Liu and Z. L. Wang, *Adv. Mater.*, 2011, **23**, 3004.
34 R. Landauer, *Philos. Mag.*, 1970, **21**, 863.
35 M. Büttiker, *Phys. Rev. Lett.*, 1986, **57**, 1761.
36 X. Luo, B. Wang and Y. Zheng, *J. Appl. Phys.*, 2009, **106**, 073711.
37 X. Luo, S. P. Lin, B. Wang and Y. Zheng, *Appl. Phys. Lett.*, 2010, **97**, 012905.